

Quantifying Improvements in Debris Risk Analysis using a Constellation of Spaceborne Optical Sensors

Antonio D'Anniballe^{a*}, Leonard Felicetti^a, Stephen Hobbs^a

^a Cranfield University, United Kingdom, antonio.danniballe@cranfield.ac.uk

* Corresponding author

Abstract

As the number of resident space objects (RSO) increases, operators face growing pressure for more accurate surveillance and collision risk analysis systems. Most of the space situational awareness domain depends today on ground-based telescopes and radar sensors, which have the disadvantage of being highly constrained in terms of their potential geographic positions. A more versatile approach may instead be using a constellation of spacecraft carrying space-based sensors. Such a distributed network of orbiting sensors can cover any desired orbital region allowing for complete coverage of RSOs, enabling a more accurate state estimation and consequent collision risk analysis. This work investigates quantitatively the benefits that an eventual network of orbiting sensors in LEO would bring to the current capabilities of the space surveillance network, in terms of improvement of the accuracy in orbit estimation of targets in LEO. A parametric analysis is carried on by varying the number of spacecraft of the constellation and their orbital parameters. Performance is evaluated in terms of accuracy on the orbit estimation and percentage of time with full coverage. The obtained results are used for preliminary evaluation of the contribution of space-based optical sensors to space surveillance systems.

Keywords: space situational awareness, orbit estimation, constellation, optical sensors

1. Introduction

In the past few years the number of launches to LEO has increased significantly. Once objects are in space, degradation and collisions with other objects causes fragmentation. The generated fragment orbit at high velocity, and may pose a risk to operational satellites. When debris are too big, they are dangerous to operators, and can contribute to the unstable evolution of the debris environment harming future missions [1]. To be able to accurately forecast the future of the space debris environment, to quantify the risks it poses, and to guarantee informative and timely conjunction data messages, it is paramount to be able to accurately determine the state of such objects at all times. Currently, objects in LEO are observed mostly through radar stations on Earth, usually part of big global ground-based space surveillance networks such the EU SST [2]. Such ground networks employ hundreds of sensors of variable size and accuracy. However, these sensors can't be deployed uniformly on Earth. Geographical and political constraints limit where a measurement station can be built, which in turns limits the timely coverage of orbital regions. Moreover, ground networks are usually the results of cooperation between many different entities that ought to closely cooperate to guarantee an effective service, a condition which is expensive to maintain and is subject to the maintaining of healthy relationships between institutions. A solution to these issues could be represented by space-based constellations of spacecraft carrying payload for space surveillance and tracking, capable of processing data, communicating with each other, and linked only to a limited number of ground stations. As there are cur-

rently some operational space surveillance spacecraft such as the Canadian Sapphire contributing to the US SSN, this solution seems technologically feasible in the near future [3].

In this paper, a study for a constellation of spacecraft carrying optical sensors for space surveillance is presented. The work focuses on evaluating the potential advantages of such a constellation when compared to a ground-based network. Moreover, the dependency of the performance of such a constellation on the constellation parameters is investigated.

In the following sections, a parametrization for the constellation is formally defined, together with a characterization of the population of debris targeted by the surveillance system, also called target population. A model for the sensors is then presented, together with the relevant assumptions. The algorithms used for orbit propagation and estimation are then discussed, along with the methodology for the parametric analysis. Results for a subset of the parameter space are then shown and discussed, providing insight on the preliminary design and potential limitations of such a surveillance system.

2. Model Definition

In this section, the analysed scenario is presented, including the assumptions for the target population and the parametrization of the sensor constellation. The sensor models are described, with a brief description of the underlying key assumptions.

2.1. Scenario

A random population of N_T targets is considered. All the targets are assumed to be objects in LEO, with altitudes between 600 and 1200 km, moving in circular orbits of random inclinations and right ascensions of the ascending node. The targets have random ballistic coefficients between 0.2 and 20 m²/kg. These are relatively high values chosen to make the effect of atmospheric drag non-negligible over short time windows.

The orbits of the targets within this population are estimated using the measurements of a constellation of spacecraft carrying optical sensors. The constellation of optical sensors is assumed to orbit the LEO region as well. The constellation assumes N_{SAT} spacecraft carrying optical sensors evenly distributed over N_o orbits in a Walker-like configuration [4]. Each orbit is assumed to be circular, at the same altitude and at the same inclination and in a radially symmetric configuration with respect to the right ascension of the ascending node. The first orbit is aligned with the ascending node. Then, for every spacecraft in the constellation:

$$in_{i,k} = in_k, i = 1 : \frac{N_{SAT}}{N_o}, k = 1 : N_o \quad (1)$$

$$raan_{i,k} = 2\pi(k-1)/N_o, i = 1 : \frac{N_{SAT}}{N_o}, k = 1 : N_o \quad (2)$$

$$\theta_{i,k} = 2\pi(i-1)N_{SAT}/N_o, i = 1 : \frac{N_{SAT}}{N_o}, k = 1 : N_o \quad (3)$$

where i is the index associated to the spacecraft within the constellation orbit, k is the index associated to the constellation orbit, in_k is the provided inclination for the constellation orbits. This parametrization is chosen to minimise the number of parameters while retaining a non-trivial set of configurations. A summary of the constellation parameters can be found in Table 1.

Table 1: Constellation Parameters

Parameter	Symbol
Number of spacecraft [-]	N_{SAT}
Number of orbits [-]	N_o
Inclination [deg]	in
Altitude [km]	h

The targets are also observed by a ground network of six radar stations mimicking existing surveillance networks such as EU SST. The precise locations used for the ground stations can be found in Table 2.

Table 2: Ground Stations

Location	Long [deg]	Lat [deg]
United Kingdom	0.0	51.0
Spain	-6.0	38.0
United States	-115.0	33.0
Chile	-69.0	-23.0
South Africa	20.0	-33.0
New Zealand	170.0	-44.0

The following assumptions hold:

- The population follows natural perturbed dynamics.
- The constellation is kept in its initial orbits via periodic station-keeping manoeuvres.
- Both the constellation and the ground network are always operational.

2.2. Sensor Models

The radar and optical sensor models are derived from purely geometrical transformations. Given a target position vector in Earth Centred Inertial (ECI) frame $\mathbf{r}_T = [x_T \ y_T \ z_T]^T$ and a sensor position vector $\mathbf{r}_S = [x_S \ y_S \ z_S]^T$, we have:

$$\rho = \sqrt{(x_T - x_S)^2 + (y_T - y_S)^2 + (z_T - z_S)^2} \quad (4)$$

$$\theta = \arccos \frac{z_T - z_S}{\rho} \quad (5)$$

$$\phi = \text{sgn}(y_T - y_S) \arccos \frac{x_T - x_S}{\rho} \quad (6)$$

where ρ is the range, θ the elevation component, and ϕ is the azimuthal component. The observation functions for the optical and the radar sensor will then be:

$$\mathbf{h}_{opt} = \mathbf{h}_{opt}(\mathbf{r}_T) = [\theta(\mathbf{r}_T) + n_\theta, \phi(\mathbf{r}_T) + n_\phi]^T \quad (7)$$

$$\mathbf{h}_{rad} = \mathbf{h}_{rad}(\mathbf{r}_T) = [\rho(\mathbf{r}_T), \theta(\mathbf{r}_T), \phi(\mathbf{r}_T)]^T \quad (8)$$

with measurement outputs:

$$\mathbf{y}_{opt} = \mathbf{h}_{opt}(\mathbf{r}_T) + \mathbf{n}_{opt} \quad (9)$$

$$\mathbf{y}_{rad} = \mathbf{h}_{rad}(\mathbf{r}_T) + \mathbf{n}_{rad} \quad (10)$$

where \mathbf{n} is a Gaussian random variable with zero mean and diagonal covariance matrix representing the noise

component of the measurement. In this work it is assumed that the standard deviation on the range $\sigma_{n,\rho}$ is 10 m and the standard deviations on the angles $\sigma_{n,\theta}$, $\sigma_{n,\phi}$ are 5 arcsec.

Measurements are only collected whenever some visibility conditions are satisfied. In particular, the target should be within the field of view of the radar sensor and illuminated by the sun such that it is visible for the optical sensors. Such conditions include:

- Visibility of target from radar sensor, expressed analytically as:

$$\arccos \frac{(\mathbf{r}_T - \mathbf{r}_S) \cdot \mathbf{r}_S}{\|\mathbf{r}_T - \mathbf{r}_S\| \|\mathbf{r}_S\|} < FOV/2 \quad (11)$$

where FOV is the field of view of the radar sensor.

- Visibility of target from optical sensor, accounting for obstruction of the Earth. Analytically [5]:

$$\sqrt{\frac{r_S^2 r_T^2 - (\mathbf{r}_T \cdot \mathbf{r}_S)^2}{r_S^2 + r_T^2 - 2\mathbf{r}_T \cdot \mathbf{r}_S}} - R_E > 0 \quad (12)$$

where R_E is the Earth radius.

- Illumination of target from the Sun, expressed as:

$$\arccos \frac{(\mathbf{r}_S - \mathbf{r}_T) \cdot (\mathbf{r}_S - \mathbf{r}_{SUN})}{\|\mathbf{r}_T - \mathbf{r}_S\| \|\mathbf{r}_S - \mathbf{r}_{SUN}\|} < \frac{\pi}{2} \quad (13)$$

where \mathbf{r}_{SUN} is the Sun-Earth vector. This expression verifies that the phase angle α , as shown in Fig. 1, is below 90 deg.

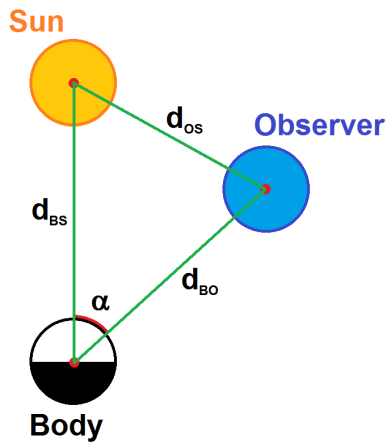


Figure 1: Phase angle for target visibility [6]

Moreover, the following assumptions hold:

- Measurements are taken continuously.

- Measurements data is sent to the ground processor for orbit estimation without delay.

- Optical payload carried by the constellation spacecraft is such that all the visible targets are captured irrespective of spacecraft attitude.

- Targets are efficiently tracked and measurement association is done instantaneously with 100% accuracy.

- The accuracy of any sensor is not dependent on range.

- All radar sensors have a high FOV of 70 deg. This takes into account the fact that a single radar station has multiple radar sensors in place to cover a broad sky area.

3. Performance Assessment Methodology

In this section, the methodology of the study is explained in detail. First, the analysed scenario is presented, including the set-up for the target population and the parametrization of the sensor constellation. First, the orbit propagation model is described. Next, the sequential orbit estimation model is presented. The algorithm for retrieving the estimation data is then explained. All the quality metrics used in the parametric analysis are defined in the following section. Finally, the algorithm for the parametric analysis is explained.

3.1. Orbit Propagation

The propagation model follows the perturbed two-body problem equations accounting for atmospheric drag and Earth oblateness effect. For an orbiting target with position vector $\mathbf{r} = [x \ y \ z]^T$, it holds [7]:

$$\ddot{\mathbf{r}} = -\frac{\mu}{r^3} \mathbf{r} + \mathbf{a}_{J_2} + \mathbf{a}_D \quad (14)$$

where μ is the Earth gravitational parameter. The perturbing accelerations are:

$$\mathbf{a}_{J_2} = \frac{3 J_2^2 E}{2 r^5} \begin{bmatrix} (5 \frac{z^2}{r^2} - 1)x \\ (5 \frac{z^2}{r^2} - 1)y \\ (5 \frac{z^2}{r^2} - 3)z \end{bmatrix} \quad (15)$$

$$\mathbf{a}_D = -\frac{1}{2} \frac{C_D A \rho}{M} v \mathbf{v} \quad (16)$$

where J_2 is the spherical harmonic coefficient of order (2,0) for the Earth's gravitational field, C_D is the drag coefficient, A is the target cross-section, M is its mass, ρ is the atmospheric density and \mathbf{v} is the velocity vector.

3.2. Unscented Kalman Filter

The orbit estimation strategy employs an Unscented Kalman Filter (UKF). Provided the known initial state and covariance for each target, one has:

$$\mathbf{x}_0 = [\mathbf{r}_0^T, \mathbf{v}_0^T]^T \quad (17)$$

where \mathbf{r}_0 is the initial position and \mathbf{v}_0 is the initial velocity of the target, with \mathbf{x}_0 initial state and \mathbf{x}_k the state at timestep t_k . An initial covariance \mathbf{P}_0 is supplied as well, such that:

$$\mathbf{P}_0 = \text{diag}(\mathbf{P}_{r,0}, \mathbf{P}_{v,0}) = \text{diag}(\sigma_{r,0}^2 \mathbf{I}_{3 \times 3}, \sigma_{v,0}^2 \mathbf{I}_{3 \times 3}) \quad (18)$$

with \mathbf{I} identity matrix, assuming $\sigma_{r,0} = 10$ m, $\sigma_{v,0} = 0.1$ m/s for all targets. Then, the UKF follows the algorithm shown in Fig. 2.

In particular, the state propagator follows a first order forward scheme, such that, given a dynamical system:

$$\dot{\mathbf{x}} = \mathbf{f}(\mathbf{x}) \quad (19)$$

for each sigma point:

$$\mathbf{x}_k = \mathbf{x}_{k-1} + (t_k - t_{k-1})\mathbf{f}(\mathbf{x}_{k-1}). \quad (20)$$

At timestep t_k , for each target, the measurement vector will contain all available measurements stacked on a single vector of size $2N$ or $3N$, depending on whether we are using the ground network or the constellation for estimation, where N is the number of available measurements, with corresponding measurement covariance of size $2N \times 2N$ or $3N \times 3N$:

$$\mathbf{y}_{const,k} = [\mathbf{y}_{opt,k}^1, \dots, \mathbf{y}_{opt,k}^N]^T \quad (21)$$

$$\mathbf{y}_{gnd,k} = [\mathbf{y}_{rad,k}^1, \dots, \mathbf{y}_{rad,k}^N]^T. \quad (22)$$

If all visibility checks fail, and therefore no measurement will be available, the Kalman gain will collapse to zero and the UKF will act as a state and uncertainty propagator.

3.3. Propagation and Estimation Function

Given the initial states \mathbf{x}_0 of all the targets, a time window t_{span} and a list of the available sensors, the algorithm for propagating and estimating the target states includes the following steps:

1. Propagate all targets using Earth oblateness and drag models.
2. Propagate all the spacecraft in the constellation using Keplerian dynamics.
3. Compute the positions of the ground sensors in ECI throughout the time window, assuming that the axis of rotation of the Earth coincides with the z-axis of the ECI frame.

4. For each target, verify for each timestep the visibility from the ground network and the constellation.
5. For each target, build the measurement vector at each timestep.
6. For each target, use UKF to estimate the target state evolution. The model used in UKF neglects the atmospheric drag.
7. Iterate over all targets.

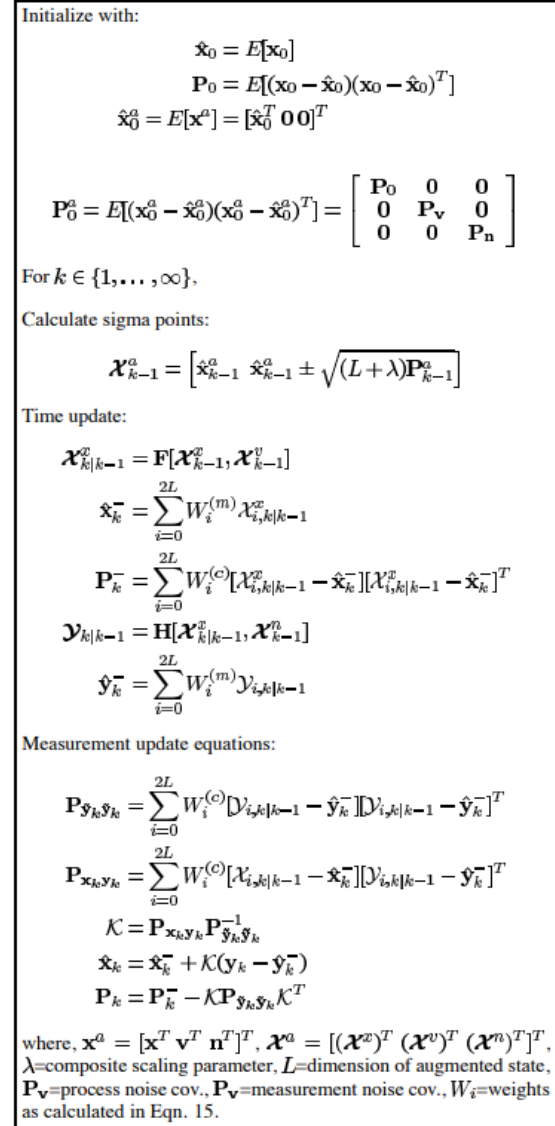


Figure 2: UKF Algorithm [8]

This algorithm is used to build up a function that maps the inputs to some meaningful outputs that are used to compute the performance metrics. These outputs are the simulated target state evolution vectors $\mathbf{x}_k(t)$, the estimated

target state evolution vectors $\mathbf{x}_{est,k}(t)$, and the number of available sensors for each target $n_k(t)$, where k is an index going from 1 to N_t , with N_t number of targets. The data is then post-processed to obtain the following quantities for each target:

- Standard deviation on position.

$$\sigma_{r,k}(t) = \sqrt{P_{xx,k}(t) + P_{yy,k}(t) + P_{zz,k}(t)} \quad (23)$$

- Uptime with at least three sensors available, that is the percentage of time for which the target is visible to at least three or more optical sensors.

$$uptime_k = \frac{\sum_{k=0}^{N_k} (n(t_k) > 2)}{N_k} \quad (24)$$

where N_k is the number of timesteps.

3.4. Performance Metrics and Parametric Analysis

From the function outputs the following performance metrics are retrieved:

- Average number of available sensors for the target population.

$$n = \text{mean}_k \text{mean}_t n_k(t) \quad (25)$$

- Average position standard deviation for the target population.

$$\sigma_r = \text{mean}_k \text{mean}_t \sigma_{r,k}(t) \quad (26)$$

- Average uptime for the target population.

$$uptime = \text{mean}_k uptime_k \quad (27)$$

These aggregate metrics are chosen as they are easily visualized and are meaningful as long as the constellation is expected to treat all targets equally.

Each parametric analysis investigates how these performance metrics depend on a variable parameter q of the constellation, keeping all the others fixed. A single parametric analysis uses a Monte Carlo method to initialize N_p different populations of N_t targets of random orbital parameters following the constraints explained in Section 2.1. Using the function in Section 3.3, for each target population one can extract $M_j(q)$, where M is a performance metric dependent on the parameter q and j is a index going from 1 to N_p . If the behaviour of the various $M_j(q)$ is very different, it means that the metric has an high dependency on the target population. By averaging over j , one can obtain the final aggregate metric $M(q)$, which is used to analyse the actual performance of the constellation over a random population.

4. Results

In this section the results for the constellation estimation function and the parametric analysis are shown and analysed for some subsets of the parameter space. The objective is to compare the performance of the constellation to the ground network for some specific target and to retrieve useful information for guiding the preliminary design of a constellation of optical sensors.

4.1. Comparison with ground network

A simulation is carried on for approximately two orbital periods for a sun-synchronous target at 98 deg inclination and 700 km altitude. The constellation is constituted by one orbit with 32 spacecraft orbiting at 70 deg inclination and 1200 km altitude. The difference between the estimated position and the simulated position is well within 3 standard deviations as it can be seen from Fig. 3, meaning that the UKF tuning was carried on correctly. It is also possible to see how the standard deviation alternates time windows of high reliability with a 100 to 400 m uncertainty with windows of exploding uncertainty.

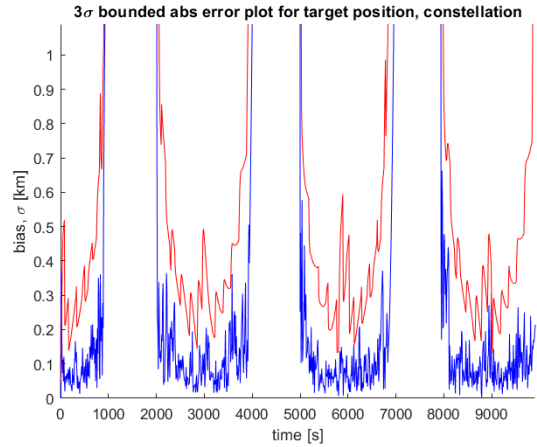


Figure 3: 3σ plot for position error and std deviation. The position error is in blue, the 3σ curve in red.

This can be explained by looking at Fig. 4, where it can be seen that the uncertainty grows exponentially whenever no measurements are available. From the same figure it possible to see how the constellation is capable of observing the target for a much higher percentage of the time window despite having all the spacecraft on a single orbit.

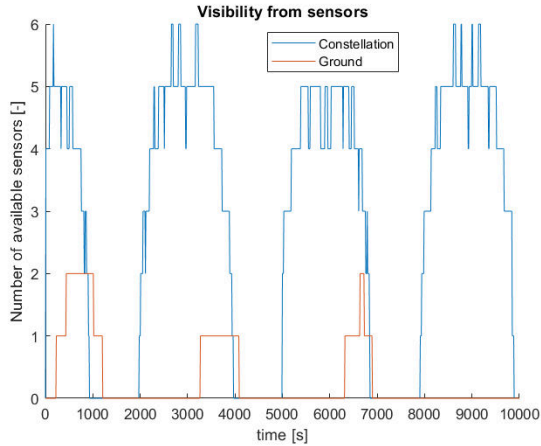


Figure 4: Available sensors against time for ground network and constellation

This yields beneficial effects, as the position is accurate for a higher percentage of the timespan as it can be seen from Fig. 5. Despite this, the same figure also shows the main disadvantage of relying on the constellation. When the measurements are available, the ground network outperforms the constellation despite having only one or two sensors at a time against four to six. This is attributable to the higher quality of information that a radar system delivers compared to an optical one, suggesting that one should be careful when choosing such systems for targeting LEO spacecraft.

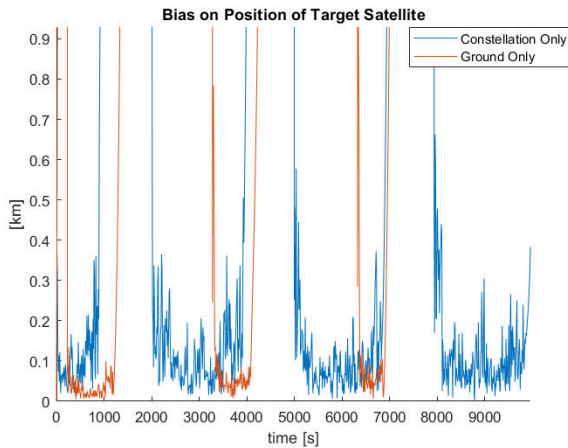


Figure 5: Position estimation error for ground network against constellation

4.2. Parametric Analysis

The parametric analysis is carried on for a target population of random inclination and right ascension of the ascending node. The number of target populations used in

the Monte Carlo analysis is 10, each composed of 25 target objects. Each analysis keeps all parameters fixed except two. The values for the fixed parameters are included in Table 3.

Table 3: Fixed parameters in the parametric analysis

Parameter	Fixed Value
Number of spacecraft N_{SAT} [-]	12
Inclination in [deg]	98
Altitude h [km]	800

In Fig. 6 it is possible to see how the average number of available sensors is independent of the number of orbits and increases linearly with the number of spacecraft. This is explained by the fact that the target population covers the sky almost uniformly, which means that the performance should be independent of the placement of the constellation spacecraft. However, this changes when looking at the uptime.

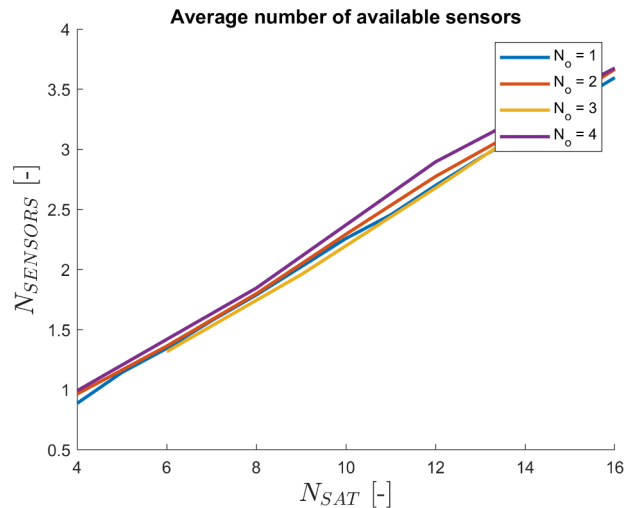
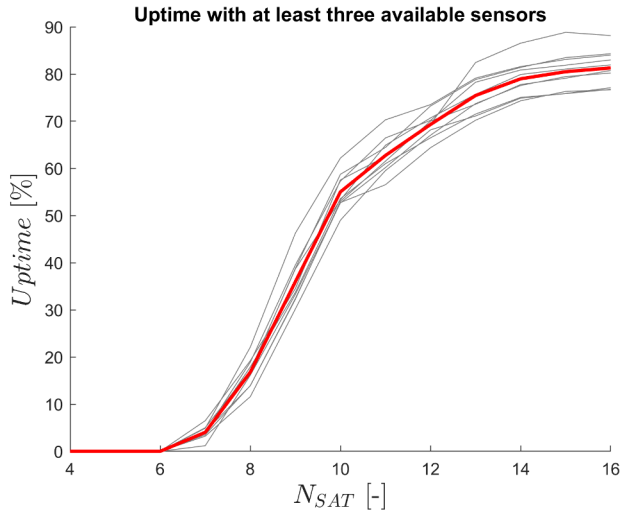
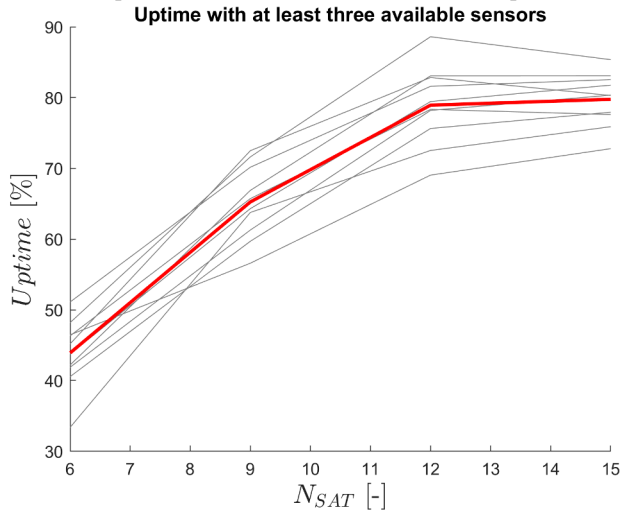


Figure 6: Average number of available sensors against number of spacecraft

Figures 7a-7b compare the uptime for 1 orbit and 3 orbits. The second case is on average better when few spacecraft are employed, although the performance is similar for a high number of spacecraft. This suggests that it is more efficient to spread out few satellites in multiple orbits to maximize effective coverage. It should also be noted that such results are largely independent of the target population, as it can be seen by how little difference is between the light grey curves.



(a) Uptime for a constellation with one orbital plane



(b) Uptime for a constellation with three orbital planes

Figure 7: Uptimes against number of spacecraft. Light grey curves indicate a single Monte Carlo run, red curves show the average over the Monte Carlo runs.

To better understand the added value brought by additional spacecraft, we may look at Fig. 8. Here the uptime is analysed with respect to the number of spacecraft per orbits $N_{SC/ORB}$. One would expect that adding more orbits would definitely improve the performance as the total number of spacecraft increases, but this is not always the case. It is noticeable how with a high number of spacecraft per orbit the performance indeed increases by increasing the number of orbits, but only by a small margin. This means that the marginal cost of the constellation does not increase linearly with the performance. Moreover, the best case is not the one with four orbits, but the one with three. This is explained by the geometry. Using three orbits covers more sky than using four, as having four orbits actually means having just two orbital

planes on which spacecraft are orbiting both in prograde and retrograde motion. This also explains why the 4 orbits case converges to the 2 orbits case for a high number of spacecraft per orbit.

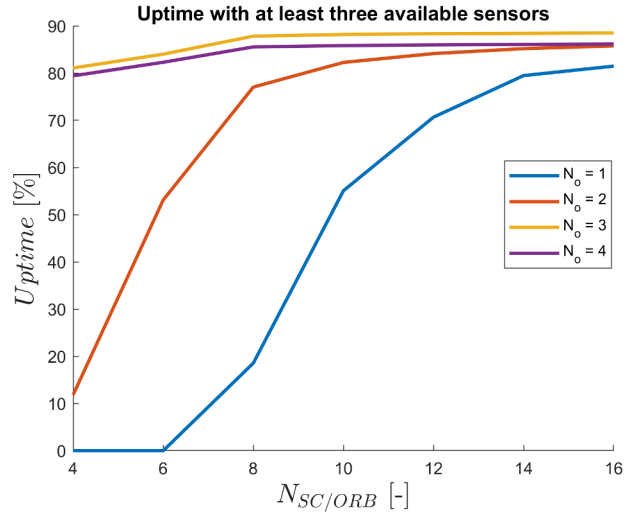


Figure 8: Uptime against number of spacecraft per orbit

This apparent paradox is even more evident when looking at the standard deviation on the position in the four cases, as shown in Fig. 9. The performance in this cases increases even less with an higher number of spacecraft. This result should however be taken carefully, as during time windows with unavailable measurements the uncertainties explode, influencing the whole metric when averaging.

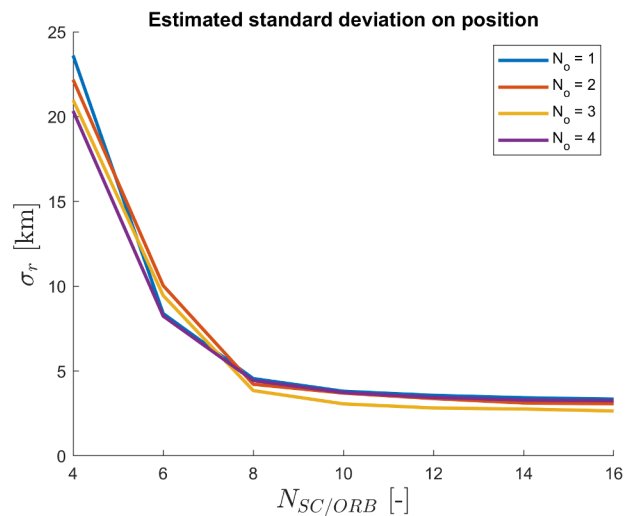


Figure 9: Position standard deviation against number of spacecraft per orbit

5. Conclusion

As more and more anthropogenic space objects are introduced in the space environment every year, potentially yielding an higher number of collisions, the need for a highly accurate space surveillance system for risk mitigation grows. Current ground based systems fare well for their accuracy and cost, but are not complete in terms of coverage and need high efforts in international cooperation to work effectively. In this paper, a potential solution of a constellation of spacecraft carrying optical payload was investigated. First, a methodology for modelling the constellation and evaluating numerically its performance was presented. To explore the advantages and limitations of such a system, both simulation for a single target object and parametric analyses over hundreds of target objects were carried on. The simulations confirmed the potential advantage of the constellation compared to a ground network of six radar stations spread over multiple continents in terms of coverage. Parametric analyses showed that performance can be reliably traced via aggregate metrics and

it is clearly dependent on the constellation parameters. However, the marginal increase in performance requires progressively more spacecraft allocated in multiple orbital planes, making such systems potentially very expensive for very high accuracies and uptimes.

In order to gain tools for designing such constellations or evaluating their contributions to a space surveillance network, much more research is required. The results of this study were limited both by the many simplifying assumptions and the limited available computing power used for performing the parametric analyses. Future research may investigate how the performance of the constellation depends on the constellation parameter for longer simulation times, for stricter and more realistic sensor assumptions, including for instance a dependency of the accuracy on the range or a limited field of view for the optical payload carried by the constellation satellites, for an higher number of target objects of different sizes, and using a model for the attitude of the constellation spacecraft.

References

- [1] ESA. ESA's Space Environment Report 2023, 2023. URL https://www.esa.int/Space_Safety/ESA_s_Space_Environment_Report_2023. Last accessed 15 September 2023.
- [2] EU SST. URL <https://www.eusst.eu/>. Last accessed 15 September 2023.
- [3] ESA. Sapphire (Space Surveillance), 2012. URL <https://www.eoportal.org/satellite-missions/sapphire-space-surveillance#sapphire-space-surveillance-mission-of-canada>. Last accessed 15 September 2023.
- [4] M. Guan, T. Xu, F. Gao, W. Nie, and H. Yang. Optimal walker constellation design of leo-based global navigation and augmentation system. *Remote Sensing*, 12(11), 2020. ISSN 2072-4292. doi: 10.3390/rs12111845. URL <https://www.mdpi.com/2072-4292/12/11/1845>.
- [5] M. E. Awad, M. A. Sharaf, and E. Khatab. Visual contact between two earth's satellites. *American Journal of Applied Sciences*, 9:620–623, 2012. URL <https://api.semanticscholar.org/CorpusID:59844610>.
- [6] Renerpho. Phase angle diagram, 2019. URL https://commons.wikimedia.org/wiki/File:Phase_angle_explanation.png. Last accessed 15 September 2023.
- [7] D. A. Vallado. Fundamentals of astrodynamics and applications. 1997. URL <https://api.semanticscholar.org/CorpusID:117909806>.
- [8] E. Wan and R. Van Der Merwe. The unscented kalman filter for nonlinear estimation. In *Proceedings of the IEEE 2000 Adaptive Systems for Signal Processing, Communications, and Control Symposium (Cat. No.00EX373)*, pages 153–158, 2000. doi: 10.1109/ASSPCC.2000.882463.

2023-10-06

Quantifying improvements in debris risk analysis using a constellation of spaceborne optical sensors

D'Anniballe, Antonio

International Astronautical Federation (IAF)

D'Anniballe A, Felicetti L, Hobbs S. (2023) Quantifying improvements in debris risk analysis using a constellation of spaceborne optical sensors. In: IAC 2023 Congress Proceedings, 74th International Astronautical Congress (IAC) 2023, 2-6 October 2023, Baku, Azerbaijan

<https://dl.iafastro.directory/event/IAC-2023/paper/79136/>

Downloaded from Cranfield Library Services E-Repository